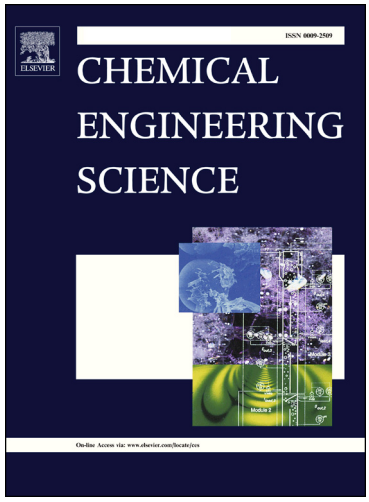

Measurement and Simulation of Mass Transfer and Backmixing Behavior in a Gas-Liquid Helically Coiled Tubular Reactor

Michael Jokiel, Lisa-Maria Wagner, Michael Mansour, Nicolas Maximilian Kaiser, Katharina Zähringer, Gábor Janiga, Krishna D.P. Nigam, Dominique Thévenin, Kai Sundmacher

PII: S0009-2509(17)30046-5
DOI: http://dx.doi.org/10.1016/j.ces.2017.01.027
Reference: CES 13373

To appear in: *Chemical Engineering Science*

Please cite this article as: M. Jokiel, L-M. Wagner, M. Mansour, N.M. Kaiser, K. Zähringer, G. Janiga, K.D.P. Nigam, D. Thévenin, K. Sundmacher, Measurement and Simulation of Mass Transfer and Backmixing Behavior in a Gas-Liquid Helically Coiled Tubular Reactor, *Chemical Engineering Science* (2017), doi: http://dx.doi.org/10.1016/j.ces.2017.01.027

Measurement and Simulation of Mass Transfer and Backmixing Behavior in a Gas-Liquid Helically Coiled Tubular Reactor

Michael Jokiel[a], Lisa-Maria Wagner[b], Michael Mansour[b], Nicolas Maximilian Kaiser[b], Katharina Zähringer[b], Gábor Janiga[b], Krishna D.P. Nigam[c], Dominique Thévenin[b], Kai Sundmacher[a,b,*]

[a]*Max Planck Institute for Dynamics of Complex Technical Systems, Sandtorstraße 1, D-39106 Magdeburg, Germany*
[b]*Otto-von-Guericke University Magdeburg, Department of Process & Systems Engineering, Universitätsplatz 2, D-39106 Magdeburg, Germany*
[c]*Indian Institute of Technology - Delhi, New Delhi 110016, India*

Abstract

Volumetric mass transfer coefficients and Bodenstein numbers (Bo) for the elongated bubble flow regime in horizontal helically-coiled tube reactors are reported using two different measurement techniques (oxygen optodes, and optical observation of an oxygen-sensitive dye). Additionally, the gas-liquid mass transfer and the residence time behavior of the two-phase flow were described with a 3D Computational Fluid Dynamics (CFD) model, and also with a one-dimensional two-phase model. For this study, 16 cases involving different gas and liquid volumetric flow rates were employed to generate air-water flows through two helically coiled tubes with curvature ratios of $\delta_1 = 0.093$ and $\delta_2 = 0.3$, respectively. The superficial gas and liquid Reynolds numbers ($\mathrm{Re}_{s,G}$ and $\mathrm{Re}_{s,L}$) and the gas hold-up (ϵ_G) are varied from 494 to 2483, from 1456 to 2713, and from 0.46 to 0.81, respectively. The mass transfer measurements show an increasing gas-liquid mass transfer rate with increasing superficial velocity of the liquid-phase and $\mathrm{Re}_{s,G}$. The Bodenstein number decreases with increasing gas-phase Reynolds number and increases with increasing superficial velocity of the liquid-phase. Correlations describing the mass transfer and backmixing behavior are proposed. The CFD results are in excellent agreement with the experimental data. With the 1D two-phase model it is possible to describe the residence time behavior of the two-phase flow through the helically coiled tube.

Keywords: helix reactor, two-phase flow, mass transfer, axial dispersion, CFD, optical measurement

1. Introduction

For continuous processes, the most often used chemical reactors are stirred tank reactors, tubular reactors and variations of these types. Due to their specific characteristics, they feature different backmixing properties. These backmixing properties are very important, since they strongly influence the performance of the reactor, namely the conversion and selectivity behavior in dependence on the underlying reaction kinetics. Moreover, if the reactants are in different state of aggregation, the backmixing behavior found in such multi-phase flows is completely different from one-phasic operation, and the mass transfer between the phases becomes an additional factor, often limiting conversion rates. In such cases, mass transfer must be enhanced by modifying the reactor geometry, e.g., by adding static mixers within tubular reactors.

It is known for a long time that the axial backmixing and mass transfer behavior of tubular reactors can be enhanced by using coiled tubes instead of straight ones (Vashishth et al., 2008). Due to coiling, the centrifugal force is induced which influence the flow and a strong secondary flow forms in radial direction, leading to Dean vortices. The secondary flow reduces axial backmixing and improves mass and energy transfer between the phases (Vashishth et al., 2008). Other advantages of the coiled configuration are its higher compactness and relatively large surface area-to-volume ratio. Additionally, the laminar flow regime in coiled tubes is observed at larger Reynolds numbers, compared to straight tubes. However, it must be kept in mind that coiling of the tube leads to an increased pressure loss (Ito, 1959; Mishra and Gupta, 1979; Ju et al., 2001).

*Corresponding author
Email address: sundmacher@mpi-magdeburg.mpg.de (Kai Sundmacher)

The present study concentrates on the backmixing properties and mass transfer in two-phase (gas/liquid) systems flowing through helically coiled tubes with the helix axis being positioned horizontally. As discussed in the next section, such systems have already been studied by other groups focusing on pressure loss (Rippel et al., 1966; Mishra and Gupta, 1979; Saxena et al., 1990; Ali, 2001; Mandal and Das, 2002; Kumar et al., 2006; Vashishth et al., 2008), heat transfer (Naphon and Wongwises, 2006; Kumar et al., 2006; Jayakumar et al., 2008; Fsadni and Whitty, 2016), or gas hold-up (Rippel et al., 1966; Saxena et al., 1990; Mandal and Das, 2002; Vashishth et al., 2008). In the present work, mass transfer and axial backmixing of air-water-flows through coiled tubes was investigated by a combination of complementary techniques: inline probes measuring oxygen absorption in water, non-intrusive optical measurements, and simulations relying on Computational Fluid Dynamics (CFD). Thanks to the combination of several powerful tools, the mass transfer and axial dispersion behavior in two-phase flows in helical coils can be better understood, opening the door for a later study involving additionally chemical reactions in this two-phase system.

2. State of the art

2.1. Mass transfer

Many studies have considered mass transfer in helically coiled tubes. Banerjee et al. (1970) studied the physical and chemical gas-liquid mass transfer of an annular flow and determined k_La-values between 0.1 $^1/_s$ and 0.47 $^1/_s$. The volumetric mass transfer coefficients k_La were correlated with the pressure loss of the coil, depending on the tube diameter. Similar measurements in the slug-flow regime were carried out in helically coiled tubes by Kulic and Rhodes (1974). These authors found k_La-values between 0.02 $^1/_s$ and 0.25 $^1/_s$ for the physical mass transfer and values between 0.22 $^1/_s$ and 0.55 $^1/_s$ for the chemical mass transfer. A comparison of the mass transfer data from Banerjee et al. (1970) and Kulic and Rhodes (1974) revealed a dependency of the mass transfer coefficient on the flow regime. Jepsen (1970) compared the physical mass transfer in helically coiled tubes and in straight horizontal tubes. The determined k_La-values in the coil were between 0.01 $^1/_s$ and 0.2 $^1/_s$. The comparison indicated a higher mass transfer rate in coiled tubes. The slightly increased mass transfer rate found in coiled tubes was confirmed by other studies (Shah and Sharma, 1973; Hameed and Muhammed, 2003; Abdel-Aziz et al., 2010; Thandlam et al., 2016) for liquid-liquid, solid-liquid and gas-liquid situations. It should be mentioned that all these studies were performed in vertically orientated coils, which is differed from the configuration used in the present investigation.

2.2. Axial dispersion and residence time distribution

For single-phase flow through helically coiled tubes it was shown that the dispersion gets reduced up to a factor of 500 compared to straight tube geometry (Trivedi and Vasudeva, 1975). However, only few studies have considered dispersion in two-phase flows (Rippel et al., 1966; Saxena et al., 1996; Sharma et al., 2017).
Rippel et al. (1966) derived general observations from experiments in a vertical coil. They noticed a similar dispersion behavior for single- and two-phase flows at liquid-phase Reynolds numbers Re_L between 400 and 2 000. At lower Re_L, the backmixing in the gas-liquid flow was higher than in single phase liquid flows.
Saxena et al. (1996) studied the residence time distribution (RTD) of an air-water flow through a vertical coil. They concluded that the curvature ratio of the coil has a negligible influence on the residence time distribution in this vertical arrangement, whereas the flow regime, which depends on the liquid flow rate, and the flow direction (upward or downward) noticeably affect the RTD.
Sharma et al. (2017) studied the axial dispersion of the liquid-phase in single- and two-phase flows depending on the expected flow regime. In stratified flows the authors observed higher axial dispersion with increasing gas-phase velocity, keeping the liquid-phase velocity fixed. The axial dispersion in the wavy flow regime was less than in the stratified flow regime. With increasing gas- and liquid-flow velocities, the annular flow regime was reached and the axial dispersion was further slightly reduced. Comparing directly single- and two-phase flows, it was observed that the dispersion in air-water flows is higher than in pure liquid flows; however, the difference becomes negligible at higher Reynolds numbers ($\mathrm{Re}_L \geq 5060$ and $\mathrm{Re}_G \geq 24350$) if the flow is out of the stratified flow regime. Additionally, Sharma et al. (2017) (horizontal coil) compared their data with the results from Rippel et al. (1966) (vertical coil) at low liquid and gas flow rates. Under such conditions, the flow fields are noticeably influenced by gravity. In horizontal coils, liquid accumulates in the lowest region of the coils, increasing backmixing. For a vertical orientation, this effect disappears.

2.3. CFD simulations

Numerous CFD investigations have considered two-phase flows in helically coiled pipes. Most of these studies focused on the hydrodynamic features, considering velocity fields, flow regimes, volume fractions, friction factor, and pressure drop (Sangani and Didwania, 1993; Kumar et al., 2006; Vashisth and Nigam, 2009; Rahimi et al., 2014; Saffari et al., 2014). More recent studies consider specifically heat transfer in such two-phase flows (Naphon and Wongwises, 2006; Rennie and Raghavan, 2006; Jayakumar et al., 2008; Ferng et al., 2012; Fsadni and Whitty, 2016). To improve heat transfer, flows of nanofluids in helically coiled pipes have been considered as well (Saamito et al., 2011; Darzi et al., 2013). Though mass transfer from the gas into the liquid-phase has been considered in a variety of two-phase flows in the literature, (e.g. Wang and Wang (2007); Wang et al. (2010); Ranganathan and Sivaraman (2011)), this problem has never been analyzed by means of detailed numerical simulation up to now in helically coiled pipes to the best of the authors' knowledge.

3. Experimental setup and procedure

Considering that horizontal coiled flow reactors have been much less investigated than their vertical counterparts, the horizontal orientation has been retained throughout this study. Previous investigations have demonstrated that, in general, the curvature ratio is the main parameter influencing hydrodynamic features in this configuration (Mishra and Gupta, 1979; Saffari et al., 2014). For this reason, two different geometries have been selected, leading to noticeably different values of the curvature ratio. The first coil geometry (abbreviated in what follows G1) leads to a curvature ratio d/D of $\delta_1 = 0.093$, while the second coil geometry (denoted G2) corresponds to a curvature ratio of $\delta_2 = 0.3$. Both geometries G1 and G2 are shown in a true-to-scale representation in Figure 1. Mixing properties associated with two-phase flows of air and water have been characterized in both geometries. For G1 (see also section 3.1) mass transfer coefficient k_La and Bodenstein number Bo have been determined using oxygen probes placed inside the helix. Configuration G2 (section 3.2), being optically transparent, allows the study of mass transfer based on non-intrusive optical observations. Since the same process conditions have been retained in both configurations, as characterized by the Dean number De_L of the liquid-phase following Mishra and Gupta (1979) and by the gas holdup ϵ_G (see Table 1), direct comparisons between both geometries

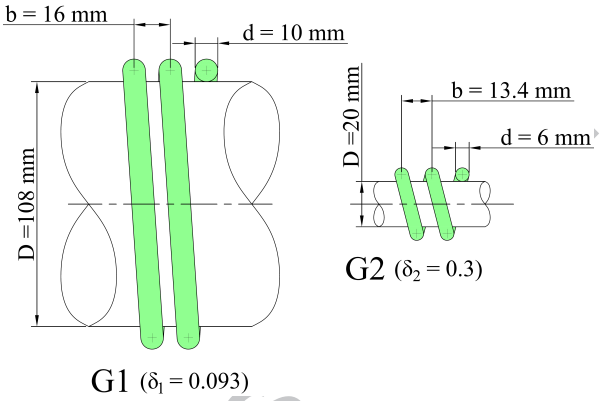

Figure 1: Geometry details for configurations G1 and G2, true-to-scale.

are possible and are presented in the discussion section.

For the measurements of mass transfer and dispersion in geometry G1, four different volume flow rates for the gas (3.3, 5.0, 10.0 and 16.6 $^{NL}/_{min}$) as well as for the liquid-phase (0.67, 0.78, 1.00 and 1.23 $^{L}/_{min}$) have been used, as presented in Table 1. The four cases written in bold in Table 1 (C1, C2, C3, C13) have been considered in both geometries G1 and G2.
The values of the minimum flow rates have been selected so that gravity has only a minor influence on the flow field and a continuous flow through the coil was observed. The maximum values of the volume flow rates are chosen to ensure that the pressure in the coil is always lower than 4 bar abs, since the employed material can only support peak pressures of 5 bar abs. A change of volumetric flow rate affects gas hold-up and pressure loss, too. To take into account all interactions between the parameters, a full factorial design of experiments was applied.

The flow regimes corresponding to all process conditions C1 to C18 (see Table 1) are represented in Figure 2 using the superficial velocities of the phases and the cross-sectional area of the coils. The marked areas indicate, that all measurements were done in the elongated bubble flow regime at the border of the stratified flow regime.

3.1. Geometry G1

3.1.1. Experimental setup

Figure 3 shows a flow chart of the experimental setup used for geometry G1. The gas flow rate was measured by two rotameters (range: 30 – 300 $^{NL}/_{h}$ for *R-1*, and 0 – 3 $^{Nm^3}/_{h}$ for *R-2*; both from KROHNE Messtechnik

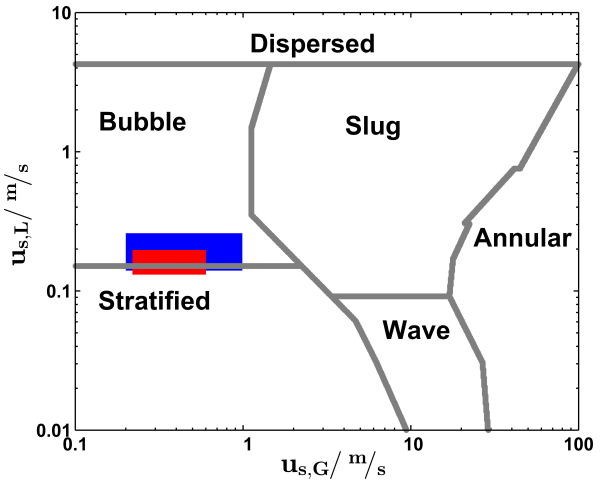

Figure 2: Flow map adopted from Mandhane et al. (1974): blue area: velocity ranges covered from measurements in configuration G1; red area: velocity ranges of the measurements in geometry G2.

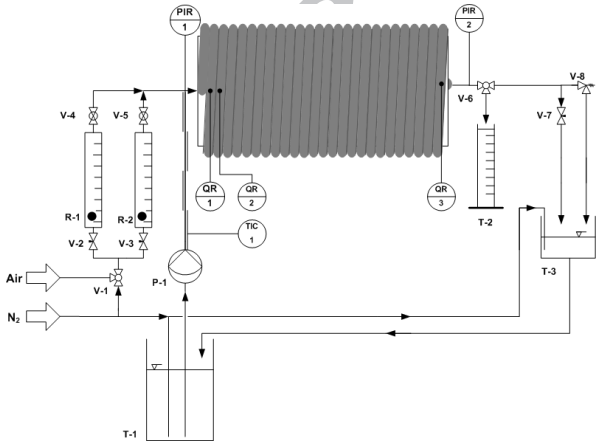

Figure 3: Experimental setup for geometry G1 using probe measurements to determine volumetric mass transfer coefficient k_La and Bodenstein number Bo.

Table 1: Process conditions employed in geometry G1. The conditions considered in both geometries (C1, C2, C3 and C13) in terms of De_L and ϵ_G appear in bold letters. (Reference values of the gas flow rate: 1.013 bar abs and 273.15 K.)

Case	Gas flow rate (NL/min)	Liquid flow rate (L/min)	De_L (-)	ϵ_G (-)
C1	3.3	0.66	**1078**	**0.630**
C2	5.0	0.66	**1370**	**0.709**
C3	10.0	0.66	**1805**	**0.779**
C6	16.6	0.66	2096	0.810
C7	3.3	0.78	1181	0.606
C8	5.0	0.78	1486	0.687
C9	10.0	0.78	2025	0.771
C10	16.6	0.78	2287	0.797
C11	3.3	1.00	1352	0.558
C12	5.0	1.00	1697	0.648
C13	10.0	1.00	**2419**	**0.753**
C14	16.6	1.00	2941	0.797
C15	3.3	1.23	1352	0.460
C16	5.0	1.23	1427	0.488
C17	10.0	1.23	2716	0.731
C18	16.6	1.23	3183	0.771

GmbH, Type VA20R) before entering the helix. The liquid-phase was fed via the piston diaphragm pump *P-1* (KNF-Lab Liquiport®1.300) from the large tank *T-1* ($V \approx 22$ L) to ensure a constant and low dissolved oxygen concentration during the measurements. At the coil inlet a T-junction was used to feed both phases into the helix. At the outlet the liquid-phase was collected in tank *T-3*, while the gas-phase escapes into the atmosphere. The water can flow from tank *T-3* back into tank *T-1*. To decrease the dissolved oxygen concentration in the liquid-phase, nitrogen was continuously bubbled in both tanks *T-1* and *T-3*. At the entrance and the exit of the coil, two pressure transducers (marked *PIR 1* and *PIR 2*, from Wika Alexander Wiegand SE & Co. KG, type CPT6200, range 0 – 6 bar), connected to a hand-held pressure device (type: CPH6200), were used to measure pressure. The pressure inside of the helix was regulated by means of the valves *V-7* and *V-8*. The liquid-phase hold-up was measured at the end of the experiments by blowing out the remaining liquid in the graduated beaker *T-2*. To ensure isothermal conditions during the measurements, tank *T-1* was additionally heated. There was also a jacketed piping between the pump *P-1* and the T-junction, which was heated with an electric heating tape. To minimize heating losses to the atmosphere, the helix was additionally insulated.

To measure the dissolved oxygen concentration, optical oxygen measurement devices (called optodes) based on fluorescent quenching (from Ocean Optics inc., type HIOXY-AL300) were used. Compared to classical

oxygen electrodes, the much smaller optodes have a faster response time, do not consume oxygen and are pressure-stable (Han and Al-Dahhan, 2007; Reis et al., 2008).

In all experiments with geometry G1, three oxygen probes were installed along the coiled tube: two in the first two coils (*QR 1* and *QR 2*), for qualifying the gas-liquid mass transfer, and a third probe (*QR 3*) in the last coil for the determination of the axial dispersion behavior. During preliminary experiments an additional optode was installed between tank *T-1* and pump *P-1* to check that a constant and low dissolved oxygen concentration was obtained in the water before entering the helix.
The G1-coil is made of thick-walled PVC with a total length of 29.28 m. The inner coil diameter, inner tube diameter, curvature ratio and coil pitch were $D = 108$ mm, $d = 10$ mm, $\delta = 0.093$ and $b = 16$ mm, respectively (see Figure 1).

3.1.2. *Determination of the volumetric mass transfer coefficient k_La*

A specific model was used for the determination of the volumetric mass transfer coefficient. For this purpose the following simplifying assumptions were made: *(i)* both phases obey plug-flow behavior and do not influence each other; *(ii)* the mass transfer between the phases can be described with the film model of Whitman (1923); *(iii)* the overall mass transfer coefficient k is approximately equal to the mass transfer coefficient of the liquid-side transport coefficient k_L; *(iv)* Henry's law can be used to describe the solubility of oxygen in water; *(v)* due to the low solubility of oxygen in water, the concentration change of oxygen in the gas-phase can be neglected; *(vi)* the pressure drop along the coil is considered as linear; *(vii)* the flow velocities, the k_La-value and the gas hold-up are constant along the coil, and *(viii)* variations in the radial direction are negligible. As a consequence of these assumptions, dispersion is not accounted for when determining mass transfer. This is supported by former studies showing that backmixing is from minor importance in coiled tube reactors (Trivedi and Vasudeva, 1975). Using all these assumptions the following mass balance can be used for the oxygen concentration in each phase $i = G, L$:

$$\frac{\partial c_i}{\partial t} = -u_i \frac{\partial c_i}{\partial z} + \Sigma_i. \tag{1}$$

The oxygen balance equations (1) are linked to each other by exchange of oxygen via gas-liquid transfer Σ_i, which is expressed as follows:

$$\Sigma_i = \nu_i \frac{k_L a}{\epsilon_i} \left(P_G K_H^{\#} - c_L \right). \tag{2}$$

Using reference values it is possible to transform Eq. (1) into a dimensionless form:

$$\Theta_i = \frac{t}{\tau_i}, \quad Z = \frac{z}{L}, \quad C_i = \frac{c_i}{c_{sat}}. \tag{3}$$

Additionally the following definitions are introduced:

$$\tau = \frac{L}{u_G \epsilon_G + u_L \epsilon_L}, \tag{4}$$

$$\tau_i = \frac{L}{\epsilon_i u_i}, \tag{5}$$

$$\Theta = \frac{\Theta_i \tau_i}{\tau}. \tag{6}$$

Eq. (4) defines the overall residence time when both phases are considered, whereas Eq. (5) defines the residence times of each phase separately. Using Eq. (6) a connection can be made between the dimensionless time scales of each phase. Now, the dimensionless form of the two-phase plug flow model can be expressed as:

$$\frac{\partial C_i}{\partial \Theta} = -\frac{\tau}{\epsilon_i \tau_i} \frac{\partial C_i}{\partial Z} + \nu_i \frac{k_L a \tau}{\epsilon_i} \left(C_G K_H - C_L \right). \tag{7}$$

The initial conditions of Eq. (7) are:

$$C_G(\Theta = 0, Z) = 0, \tag{8a}$$

$$C_G(\Theta, Z = 0) = \frac{P X_{O_2}}{R\ T\ c_{sat}}, \tag{8b}$$

$$C_L(\Theta = 0, Z) = \frac{c_{L,\,inlet,exp.}}{c_{sat}}, \tag{8c}$$

$$C_L(\Theta, Z = 0) = \frac{c_{L,\,inlet\ exp.}}{c_{sat}}. \tag{8d}$$

The model described by Eq. (7) has been fitted to the dissolved oxygen profiles measured experimentally by means of the optodes *QR 1* and *QR 2*, using the k_La-value as the only fit parameter. As a measure for the agreement between model and experimental data, the coefficient of determination $1 - R^2$ was used. The fitting is done with the *fminsearch*-function of the optimization toolbox in *MATLAB*.

3.1.3. Determination of the Bodenstein number Bo

A common model to describe the backmixing behavior of real chemical reactors is the axial dispersion model (Levenspiel, 1998; Baerns et al., 2006), described by Eq. (9) for nonreactive single-phase conditions:

$$\frac{\partial C}{\partial \Theta} = \mathrm{Bo}\frac{\partial^2 C}{\partial \Theta^2} - \frac{\partial C}{\partial Z}. \tag{9}$$

However, Eq. (9) can only be solved analytically, if the reactor is open on both sides for the dispersion (Baerns et al., 2006). Since the tube diameter at reactor inlet and outlet does not change, and considering the length of the employed tube (L = 29.28 m), this boundary condition is suitable in our case. However, the analytical solution of Eq. (9) is not very sensitive to changes of the Bodenstein number. Therefore, trying to fit the dispersion model described by Eq. (9) to the obtained experimental data failed. For this reason, alternative solutions of Eq. (9) proposed in the scientific literature were used to determine the Bodenstein number:

- For Bo > 50 the cumulative distribution can be calculated as follows (Hofmann, 1961):

$$F(\Theta) = \frac{1}{2}\left[1 - \mathrm{erf}\left(\frac{\sqrt{\mathrm{Bo}}\,(1-\Theta)}{2\sqrt{\Theta}}\right)\right]. \tag{10}$$

- For Bo > 100 the reactor behaves like an ideal plug flow reactor for which the age distribution function can be determined as follows (Levenspiel, 2012):

$$E(\Theta) = \sqrt{\frac{\mathrm{Bo}}{4\pi}} \cdot \exp\left[-\frac{1}{4}(1-\Theta)^2\mathrm{Bo}\right]. \tag{11}$$

- For Bo < 100 the age distribution function can be expressed as follows for open boundary conditions (Baerns et al., 2006; Levenspiel, 2012):

$$E(\Theta) = \left(\sqrt{\frac{4\pi\Theta}{\mathrm{Bo}}}\right)^{-1} \cdot \exp\left[-\frac{(1-\Theta)^2\,\mathrm{Bo}}{4\,\Theta}\right]. \tag{12}$$

It should be mentioned that the employed boundary conditions are only important for Bo < 100 (Baerns et al., 2006). For higher Bodenstein numbers, all solutions become similar to each other, independently from the special type of boundary conditions.

The least-square error method was used to minimize the error between the experimental data and the profiles from Eqs. (10), (11) and (12). Therefore, the *MATLAB*-solver *fminbnd* was used with the Bodenstein number as fitting parameter.

Experimentally, a pulse signal was realized by switching first the gas flow from air to nitrogen and, at the time t = 0 s, switching back instantaneously from nitrogen to air. Due to backmixing, the response becomes wider in space while the signal travels trough the coil. The data from the oxygen probe *QR 3*, located at the coil outlet, are finally used to measure the dispersion behavior of the helically coiled tube.

3.1.4. Consideration of the probe response time

For dynamic measurements, it is very important to consider the response time of the probe (Merchuk et al., 1989; Malgorzata and Piotr, 2014). It should first be noticed that the probe response time had no influence on the determined volumetric mass transfer coefficients, since steady-state conditions were used. Therefore, the probe response time was only important for studying axial dispersion. For dynamic measurements of the axial dispersion coefficient, no recommendation could be found in the literature concerning appropriate probe response times. Therefore, recommendations for the determination of the volumetric mass transfer coefficients have been used. Here, we used the recommendation that $^1/_{k_La}$ should show the same order of magnitude as the response time of the probe (Grachia-Ochoa and Gomez, 2009). τ_{Probe} is defined as the time lag when the measured value reaches 63% of its final value, if the probe is exposed to a step change of concentration. The response time τ_{Probe} of each probe was determined via switching the probes from a beaker of water without dissolved oxygen (nitrogen bubbling) into a beaker with oxygen-saturated water. The response time can be approximated using a first-order kinetic (Grachia-Ochoa and Gomez, 2009):

$$\frac{dc_{Probe}}{dt} = \frac{[c_L(t) - c_{Probe}(t)]}{\tau_{Probe}}. \tag{13}$$

The determined probe response times are $0.93\ \mathrm{s} \leq \tau_{Probe} \leq 1.28\ \mathrm{s}$. The probe with the smallest τ_{Probe} is used for the dispersion measurements in position *QR 3*.

3.2. Geometry G2

3.2.1. Experimental setup

In this configuration mass transfer from the gas-phase to the liquid-phase was observed optically, via the so-called blue bottle reaction. Methylene blue was used as an oxygen-sensitive dye, as presented in Mills (2005). Adding oxygen to an initially oxygen-free mixture of

methylene blue, sodium hydroxide and glucose, the solution turns blue. This is due to a redox reaction, represented in Figure 4, where the reduction of methylene blue from blue to clear occurs parallel to the oxidization of glucose to gluconate. Adding oxygen leads to an oxidization of the clear methylene blue solution and it gets blue again. A solution of 5 $^{g}/_{L}$ NaOH, 40 $^{g}/_{L}$ glucose and 10 $^{mg}/_{L}$ methylene blue was used for our study. The intensity of the blue color is an indirect measure of the dissolved oxygen, varying between the extreme values I_o (original, low value) and I_f (final, high value). The progress of mass transfer from the gas to the liquid phase could thus be measured indirectly, using the non-dimensional progress variable computed from the local intensity I of the blue color in the image:

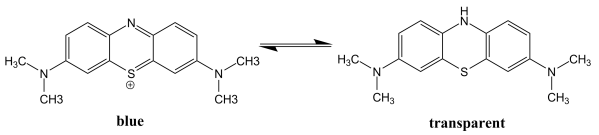

Figure 4: Structure of the oxidized state of methylene blue (blue, left), and of the reduced state (transparent, right).

$$\overline{c} = \frac{I - I_o}{I_f - I_o}. \tag{14}$$

The progress variable varies from $\overline{c} = 0$ (no oxygen dissolved) to $\overline{c} = 1$ (saturation reached).
For investigating optically the mass transfer, a transparent helical coil made of glass with an inner tube diameter of $d = 6$ mm, an inner coil diameter of $D = 20$ mm, a pitch of $b = 13.4$ mm (see G2 in Figure 1) with 15 coils has been mounted within a box made of PMMA and filled with glycerol. Thanks to this arrangement, differences in refractive index can be minimized, allowing high-quality optical measurements.
The water solution containing the oxygen-sensitive dye was pumped through the helix with a micro-gear pump (Watson Marlow, Model 5003 U Issue 1). Before entering the coil, air was fed through a T-junction using a mass flow controller (Bronkhorst, Model: EL-FLOW). The pipe between the T-junction and the first coil was 13 cm long and had an inner diameter of 6 mm.
3000 images were recorded with a high-speed camera (ImagerPro from LaVision) using a 105 mm-objective and a recording rate of 100 Hz. Illumination was provided by a 40 W LED-lamp and a white background was used as diffusor.

3.2.2. Processing of the images

All images were processed using the software *DaVis* from *LaVision*.
First, 50 images of clear water and of the saturated (blue) solution were separately averaged to use them as sheet image in the further process, and to obtain the values of I_o and I_f.
The raw images were divided by the clear image to correct the influence of illumination. Two different mask functions were then applied to extract the liquid zones and exclude the bubbles from postprocessing within the raw images. The 3000 images were finally averaged to a mean image, as illustrated in Figure 5. To measure the intensity change and therefore the mass transfer from oxygen to water, the intensity of each coil of the helix was averaged. The resulting profiles of $\overline{c}$ were computed with Eq. (14), using the profiles of the blue and clear images processed in the same manner.

4. Numerical modeling

4.1. Mathematical modeling of backmixing

The axial dispersion model described by Eq. (15) can be used as starting point to describe the dispersion behavior under noreactive gas-liquid conditions (Hofmann, 1961; Levenspiel, 1998):

$$\frac{\partial c_i}{\partial t} = D_{ax}\frac{\partial^2 c_i}{\partial z^2} - u_i\frac{\partial c_i}{\partial z} + \Sigma_i. \tag{15}$$

The two mass balances for $i = G, L$ are linked to each other via the source and sink term, Eq. (2).
Again, the model can be transformed into a dimensionless form. For this purpose, the same reference values, Eq. (3), as for the plug flow model, Eq. (7), were used. Additionally, the Bodenstein number ($\mathrm{Bo}_i = u_i L/D_{ax}$) is required. With the help of Eqs. (4), (5) and (6), the dimensionless form of the dispersion model can be formulated as:

$$\frac{\partial C_i}{\partial \Theta} = \frac{\tau}{\tau_i\,\epsilon_i}\left[\frac{1}{\mathrm{Bo}_i}\frac{\partial^2 C_i}{\partial Z^2} - \frac{\partial C_i}{\partial Z}\right] + \nu_i\frac{k_L a\,\tau}{\epsilon_i}\left(C_G K_H - C_L\right). \tag{16}$$

For solving the axial dispersion model, Eq. (16), first it has to be discretized with respect to the spatial coordinate Z. This was done by use of the finite-volume method to naturally enforce conservativity. The initial and boundary conditions read:

$$C_G(\Theta = 0, Z) = 0, \tag{17a}$$

$$C_G(\Theta, Z = 0) = \frac{P X_{O_2}}{R\,T\,c_{sat}}, \tag{17b}$$

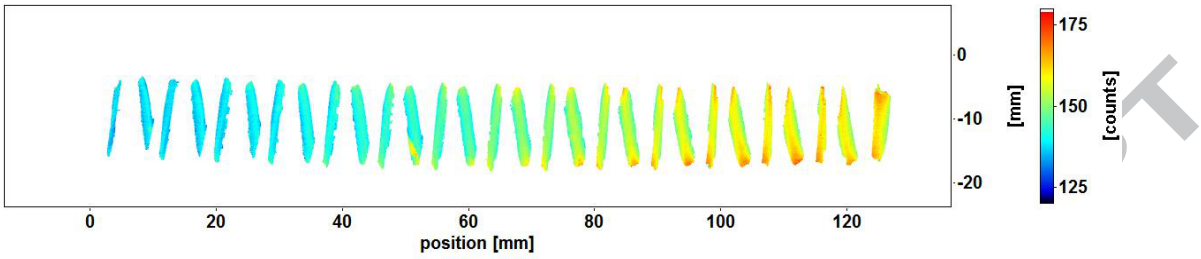

Figure 5: Emission intensity (a.u.) in the masked and averaged image obtained from 3000 raw images for case C1 in the helix reactor of geometry G2, with flow from left to right.

$$\left.\frac{dC_G}{dZ}\right|_{Z=1} = 0, \tag{17c}$$

$$C_L(\Theta = 0, Z) = \frac{c_{L,\,inlet,exp}}{c_{sat}}, \tag{17d}$$

$$C_L(\Theta, Z = 0) = \frac{c_{L,\,in\,exp.}}{c_{sat}}, \tag{17e}$$

$$\left.\frac{dC_L}{dZ}\right|_{Z=1} = 0. \tag{17f}$$

The resulting discretized axial dispersion model was finally solved with the ODE-solver *ode15s* in *MATLAB*.

4.2. Computational Fluid Dynamics

The industrial CFD code *Star-CCM+* (CD-Adapco) was employed in the present investigations to simulate flow hydrodynamics and mass transfer within the helical pipe. The software is based on the finite-volume method for solving all relevant transport equations. Figure 6 shows details of geometries G1 and G2 with the corresponding meshes used for discretization. In all simulations, a hexahedral mesh was used with a total number of almost 2 million and 0.6 million cells for G1 and G2, respectively, leading to grid-independent results. Three or four coils are considered in the simulations for configurations G1 and G2, respectively, which is sufficient to compare the dissolved oxygen concentration with the measured values of the oxygen optodes placed at the end of the first and second coils. Additionally, in the light of previously published studies, the flow reaches both thermally and hydrodynamically fully developed conditions within the first two coils (Austin and Seader, 1975; Ferng et al., 2012; Saffari et al., 2014). The inlet mass flow rates correspond to the values retained in the corresponding experiments. The segregated, unsteady, implicit solver was used with a time step of 1 ms and a total number of inner iterations of 15. The solution was considered as converged when the residuals of the conservation equations went below 10^{-6}. To model the interaction between the air and the water phases, the Volume

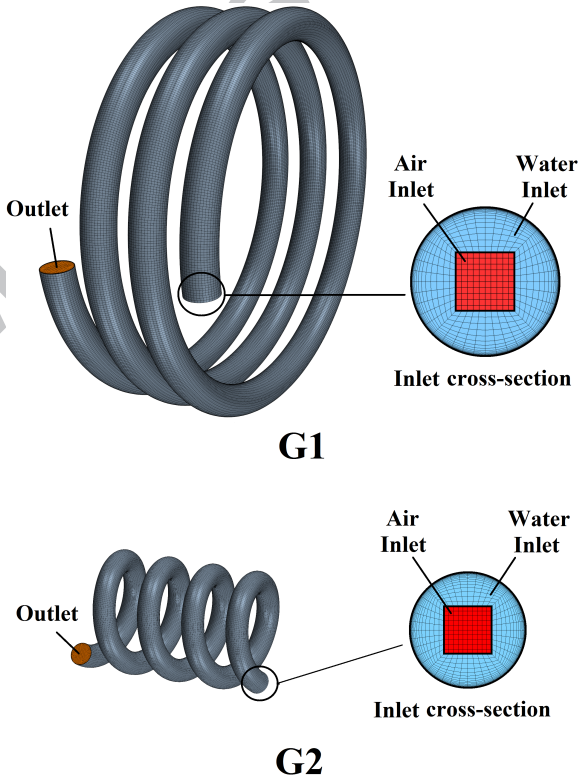

Figure 6: Geometry and typical mesh for configurations G1 and G2 in the CFD-simulations.

of Fluid (VOF) model was employed. VOF assumes common velocity, pressure and temperature fields for the two phases. This model is appropriate when the grid size is small enough compared to the phase interface length. Both phases were considered to have constant densities (incompressible flow). The surface tension between water and air was taken into account with a constant value of 0.072 $^{N}/_{m}$. The air phase was defined as a two-component gas with 21% of oxygen and 79% of nitrogen by mole. Since it corresponds to the

measurement data, oxygen was considered as the only gas dissolving into the liquid. The measured values of the already dissolved oxygen in the inlet water in the experiments were also taken into account in the simulations.

The Gas Dissolution Model implemented in *Star-CCM+* was used to predict the mass transfer between the phases (Sauer, 2000). This model calculates the amount of dissolved gas into a liquid based on Henry's law, using a homogeneous seed-based approach. The method has been extended in *Star-CCM+* (CD-Adapco) to model general gas-liquid mass transfer for gas dissolution, cavitation, and boiling processes. This model contains a single free parameter controlling gas dissolution rate, the number density of bubble seeds n_o, relating the volumes of gas and liquid (V_G and V_L), respectively. The basic equations of the model are:

$$\frac{V_G}{V_L} = \frac{4}{3}\pi r^3 n_o, \tag{18}$$

$$\epsilon_G = \frac{V_G}{V_G + V_L} = \frac{\frac{4}{3}\pi r^3 n_o}{1 + \frac{4}{3}\pi r^3 n_o}, \tag{19}$$

where r is the average bubble radius, that can be expressed as:

$$r^3 = \frac{3\epsilon_G}{4\pi\epsilon_L n_o}. \tag{20}$$

Finally, the mass transfer (gas dissolution) rate per unit volume is expressed as:

$$\dot{m} = 4\pi r^2 n_o \rho_G \epsilon_L \frac{dr}{dt}. \tag{21}$$

The term $\frac{dr}{dt}$ is calculated based on the Epstein-Plesset formulation (Epstein and Plesset, 1950):

$$\frac{dr}{dt} = \frac{D_L\,(C_{L\,\mathrm{sur}} - C_{L\,\mathrm{bulk}})}{\rho_G r}. \tag{22}$$

Hence, $\dot{m}$ can be rewritten as:

$$\dot{m} = 4\pi r n_o \epsilon_L D_L (C_{L\,\mathrm{sur}} - C_{L\,\mathrm{bulk}}). \tag{23}$$

Comparing the simulation results with our experimental data obtained in geometry G1, a linear relationship between n_o-values and gas volume fractions has been found, leading to a very good agreement (see later Figure 13). Thus, following linear relation has always been used to set the value of n_o:

$$n_o = (3.19\epsilon_G - 2.11) \cdot 10^9. \tag{24}$$

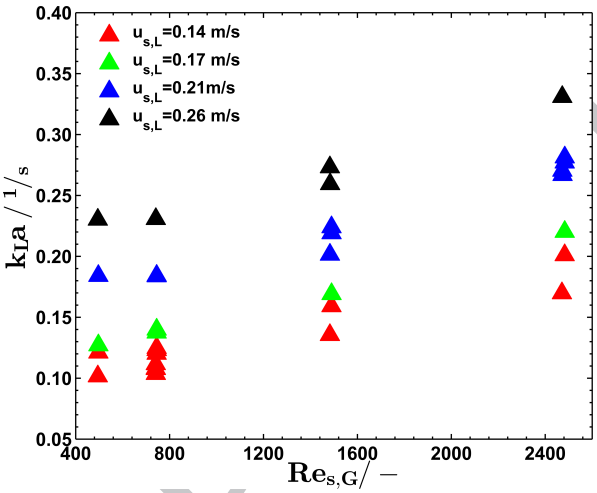

Figure 7: Measured volumetric mass transfer coefficients k_La as function of the superficial Reynolds number of the gas-phase.

5. Results

5.1. Oxygen probe measurements in geometry G1

5.1.1. Mass transfer behavior

Figure 7 shows the measured volumetric mass transfer coefficients k_La as function of the superficial Reynolds number of the gas-phase. The experimentally determined k_La-values of the helically coiled tube in horizontal position lie between 0.1 $^1/_s$ and 0.33 $^1/_s$. At low gas-phase Reynolds numbers ($450 \leq \mathrm{Re}_{s,G} \leq 850$) k_La-values stay nearly constant. Above this limit ($\mathrm{Re}_{s,G} > 850$) mass transfer rate increases noticeably with $\mathrm{Re}_{s,G}$. In all cases, an increase of the mass transfer rate with increasing liquid-phase flow rate (quantified with $u_{s,L}$ in Figure 7) is clearly visible, with a linear trend.

The values determined in this study are in a good agreement with previously published results. They are for instance similar to the values from Kulic and Rhodes (1974), which is expected since both investigations were performed in the same flow regime based on the flow map from Sharma et al. (2017).

The volumetric mass transfer coefficient is often correlated with the energy dissipation. Deriving energy dissipation from pressure loss through the Euler number ($\mathrm{Eu}_L = \Delta P_{TP}/\rho_L {u_{s,L}}^2$), a coefficient of determination of only $R^2 \approx 0.71$ was obtained between the experimental data and the correlation. Due to the influence of many physical processes it is impossible to derive directly simple dependencies using the Buckingham-Π-theorem. Considering the most important non-dimensional numbers in the correlation, the best fit was

finally achieved with the following equation:

$$\frac{k_L a\, L}{u_{s,L}} = \mathrm{Re}_{s,L}^{1.15}\mathrm{Re}_{s,G}^{0.19}\left(\frac{d}{D}\right)^{1.76}\mathrm{Eu}_L^{0.66}. \qquad (25)$$

The coefficient of determination of Eq. (25) is now $R^2 = 0.91$. The range of validity of Eq. (25) is $494 \leq \mathrm{Re}_{s,G} \leq 2483$, $1456 \leq \mathrm{Re}_{s,L} \leq 2713$, $0.0093 \leq \mathrm{Eu}_L \leq 0.0345$; $^d/_D = 0.9273$.

5.1.2. Axial dispersion behavior

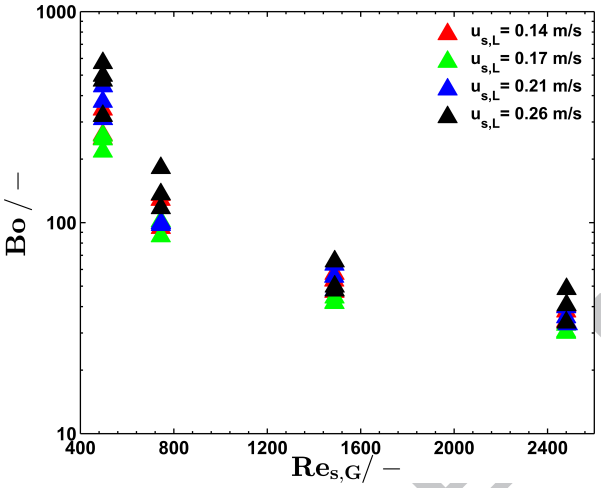

Figure 8: Determined Bodenstein numbers Bo as a function of the superficial Reynolds number of the gas-phase.

The Bodenstein numbers determined from the experimental data are shown in Figure 8. The Bodenstein numbers decrease very rapidly with increasing gas-phase Reynolds number. At the same time, Bo increases with the superficial velocity of the liquid-phase, particularly at low values of $\mathrm{Re}_{s,G}$, while the influence of $u_{s,L}$ becomes small at high values of the gas-phase Reynolds number.

Compared to previous studies (Sharma et al., 2017; Rippel et al., 1966), the observed trends are surprising at first. However, these previous studies have only investigated the liquid component of the two-phase flow. In the present study a gas-phase tracer is used instead to study the dispersion behavior within the coil. Hence, the present results must be seen as a quantification of the overall dispersion behavior within the two-phase flow, and not just of the liquid-phase.

Here again, it is not possible to get directly a simple correlation from the Buckingham-Π-theorem. Using the previously employed dimensionless numbers the following correlation shows the best agreement with the measurement data ($R^2 = 0.93$):

$$\mathrm{Bo} = 40.4 + \mathrm{Re}_{s,L}^{1.13}\mathrm{Re}_{s,G}^{-3.48}\left(\frac{d}{D}\right)^{-7.84}. \qquad (26)$$

The range of validity of Eq. (26) is $495 \leq \mathrm{Re}_{s,G} \leq 2486$, $1577 \leq \mathrm{Re}_{s,L} \leq 2959$ and $^d/_D = 0.9273$. The influence of the Euler number was found negligible.

5.2. Results from optical measurements in geometry G2

As presented previously in Table 1, four process conditions have been considered in geometry G2. The streamwise evolution of the progress variable $\bar{c}$ along the axial direction as a function of the number of coils for the four process conditions investigated in geometry G2 are shown in Figure 9. Combining this information

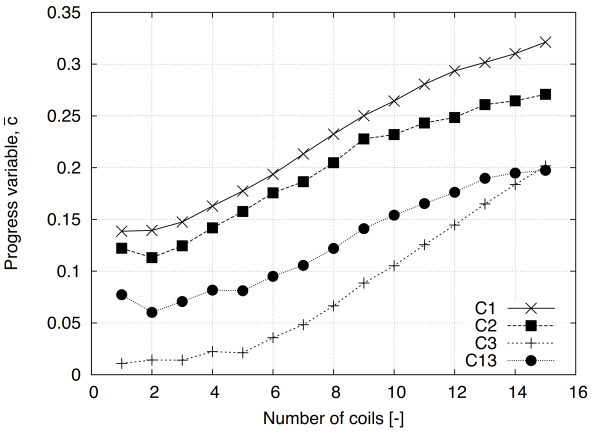

Figure 9: Evolution of the progress variable $\bar{c}$ in space along the helix reactor as a function of number of coils, for the four process conditions investigated in geometry G2.

with the mean fluid transport velocity within the helix reactor derived from the employed volume flow-rates and tube diameter, the streamwise position in Figure 9 can be converted into an equivalent residence time. As a consequence, it is possible to plot again Figure 9 with the residence time within the helix reactor as horizontal axis, as shown in Figure 10. Due to the different transport velocities associated to the different process conditions, the length of this time coordinate is now specific to each configuration. A characteristic time $\bar{\tau}$ associated to the reaction within the helix reactor can now be computed for each case. Due to the fast oxidation of methylene blue, this characteristic reaction time is expected to characterize as well the oxygen mass transfer from the gas to the liquid phase, since this is the limiting process. Two different approaches have been selected to compute this characteristic time:

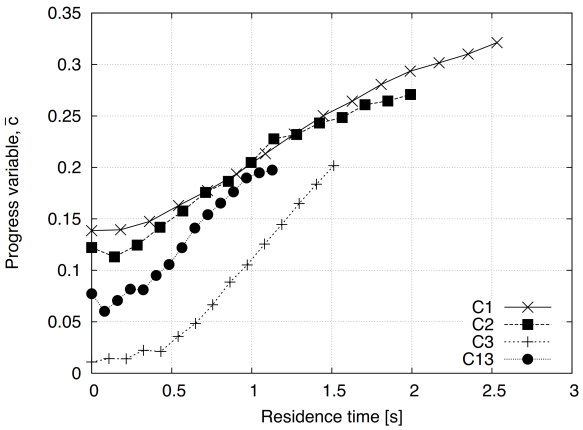

Figure 10: Evolution of the progress variable $\overline{c}$ as a function of residence time within the helix reactor, for the four process conditions investigated in geometry G2.

1. The integral time $\overline{\tau}_I$ is obtained by dividing the residence time within the reactor (the final time appearing in Figure 10 for one specific case) by the associated change in progress variable $\Delta\overline{c}$ (the vertical direction spanned by the curve in Figure 10).
2. The fastest time $\overline{\tau}_F$ corresponding to the inverse of the steepest slope in Figure 10.

The corresponding values of $\overline{\tau}$ are listed in Table 2 and show as expected a similar behavior. The corresponding values of $\overline{\tau}$ are listed in Table 2 and show as expected a similar behavior.

Table 2: Characteristic times describing the oxygen mass transfer obtained indirectly from optical measurements in geometry G2.

Case	Integral time $\overline{\tau}_I$ (s)	Fastest time $\overline{\tau}_F$ (s)
C1	13.9	11.3
C2	13.4	11.5
C3	7.93	5.61
C13	9.40	5.71

5.3. Numerical modeling results

5.3.1. Mathematical model

The two phase dispersion model given by Eq. (16) was used to model the residence time distribution (RTD) behavior of the coil. For this, two variants of the model have been tested. In model I the dispersion in the gas-phase is neglected ($\mathrm{Bo}_G = 0$), whereas model II considers the dispersion in both phases ($\mathrm{Bo}_i \neq 0$). Neglecting the dispersion in the gas-phase seems at first reasonable due to relatively high Bodenstein numbers, together with practical guidelines in reactor design stating that one can neglect the dispersion behavior for Bo > 100 (Baerns et al., 2006). Figure 11 shows the comparison of the modeled RTDs and the experimental profile for an experiment with a strong contribution of dispersion ($\mathrm{Bo}_L = 61$). From the cumulative distribution functions on the left hand side of Figure 11 one can see that the agreement of model I with the experimental profile is poor; model I predicts a much smaller dispersion than measured in the experiment. However, the agreement between model II and the experimental cumulative distribution is quite good.

The right hand side of Figure 11 shows the derived curves of the cumulative distributions of the left hand side. For the derivation of the experimental profile, the curve had to be further smoothed. The figure shows again the bad agreement of model I with the experimental profile. The agreement between the E(Θ)-curve of model II and the experimental profile is better, but due to the nonsymmetrical experimental profile not excellent. However, one has to keep in mind, that the used models contain only one fitting parameter to describe the axial dispersion. Therefore it should be possible to describe the RTD-behavior better with the usage of a compartment model with more parameters. As a first approximation the simple model can describe the residence time behavior of the coil quite well.

In the case of low dispersion, both models show good agreement with experimental data, even though model II slightly overestimates the dispersion. Analyzing all data for a variety of Bo-values, it was found that the dispersion should be taken into account in both phases if the Bodenstein number is smaller than 140. For higher values of Bo it is sufficient to consider the dispersion in the liquid phase only.

5.3.2. Computational Fluid Dynamics

In the CFD simulations three different conditions have been investigated in each geometry. Referring to Table 1, conditions C2, C13 and C18 were simulated for geometry G1, while C2, C3 and C13 have been considered in geometry G2. The obtained volume fraction of air and dissolved oxygen concentration for condition C2 are shown for both geometries in Figure 12 after simulating 10 s of physical time, which is sufficient to reach statistically-steady conditions. From these results, it is clear that the flow experiences the same flow regime in both geometries, as expected since non-dimensional parameters are the same (look again at Figure 2). However, the amount of dissolved oxygen is considerably higher in G1 compared to G2, which can

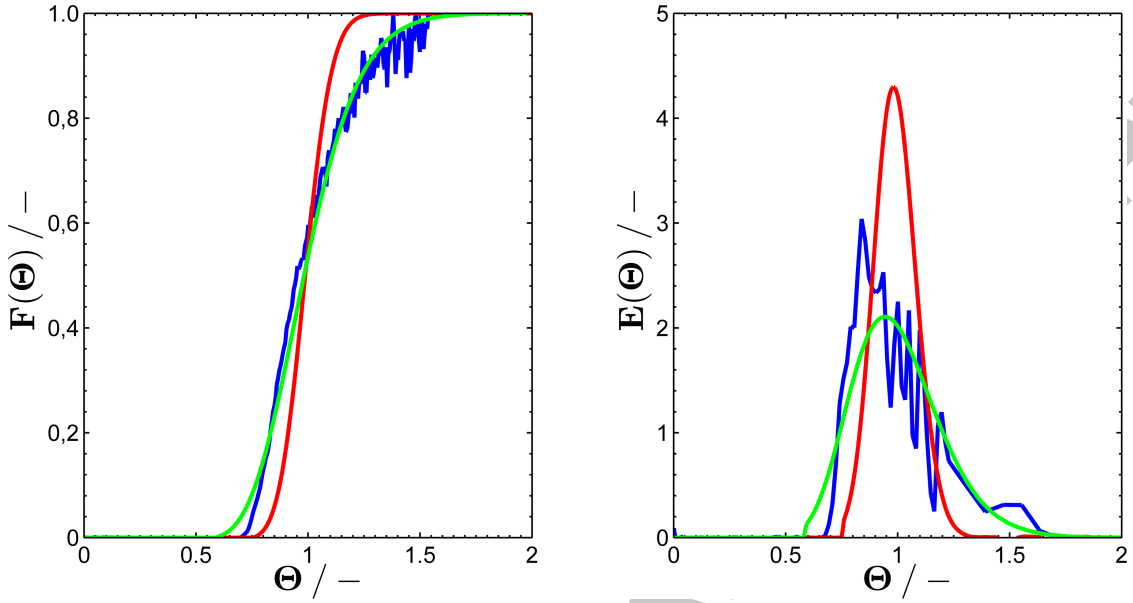

Figure 11: Cumulative distribution function (left hand side) and age distribution function (right hand side) of the experimental residence time behavior (blue line); model I (red line) and model II (green line).

easily be explained by the difference in pressure (different solubility limits) and in size (see again Figure 1) between both configurations. Figure 13 shows the evolution of the time-averaged dissolved oxygen concentration along the developed length of the helix reactor. For all simulations the CFD results are in very good agreement with the values measured by the oxygen probes (shown as triangles in Figure 13) at the end of the first and the second coil of G1, the R^2-correlation values are better than 0.9895 in all three cases. Figure 13 also indicates that the dissolved oxygen concentration depends on the position (top/side/bottom) within one coil, due to the influence of gravity in this two-phase flow.

6. Discussion

The mass transfer behavior has been studied in both geometries. A general comparison of Figure 7 and Figure 9 shows that the mass transfer rate increases with increasing gas hold-up. It was also noticed in both geometries that the mass transfer rate increases with increasing volume flow rates of the gas- and liquid-phase, using residence time as a coordinate. From the CFD study in Figure 13 it can be seen for the cases C2 and C13 that dissolved oxygen concentration in G2 increases only slightly, whereas the dissolved oxygen concentrations in G1 increases strongly. There is no noticeable difference in the increase of dissolved oxygen concentration between the employed cases (C2, C3 and C13) in G2

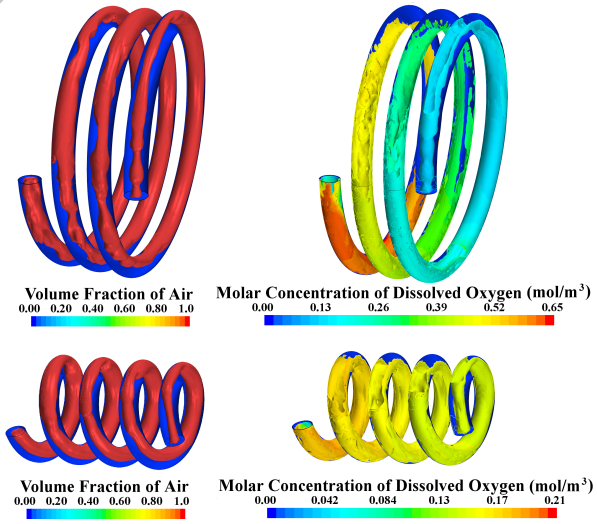

Figure 12: Air volume fraction and dissolved oxygen concentration obtained by CFD for Geometries G1 (top) and G2 (bottom) and condition C2. Note the different color scales.

(Figure 13) visible. Based on this observation, curvature ratio and pressure have a big influence on the mass transfer behavior.

This study has been carried out only in the elongated bubble flow regime. To the knowledge of the authors, no study has been published concerning the influence of the flow regime on the gas-liquid mass transfer under

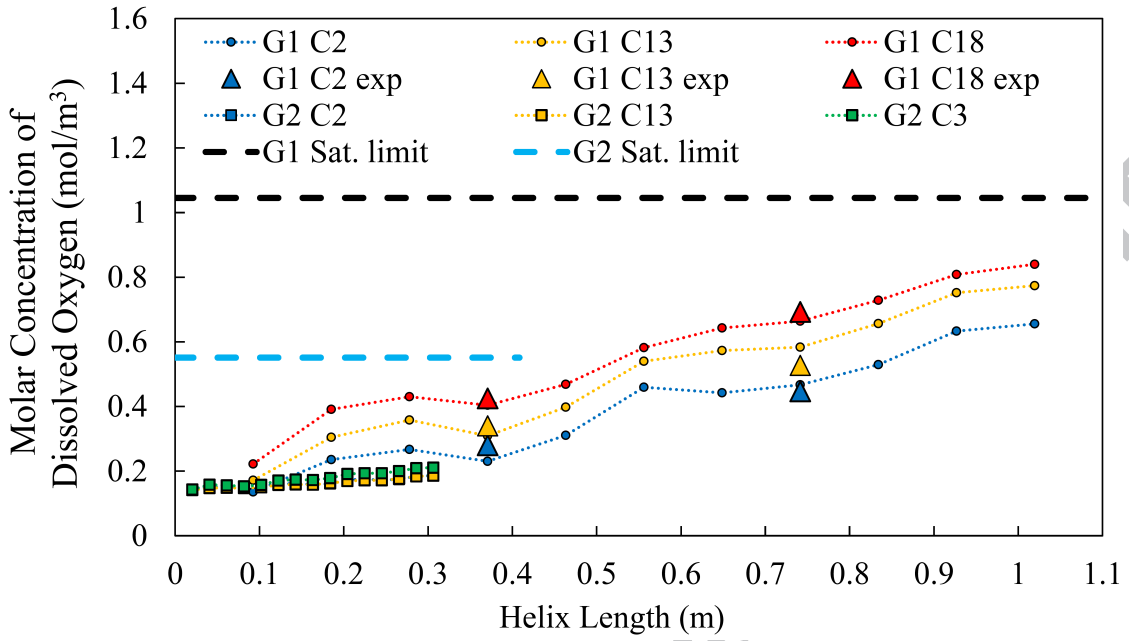

Figure 13: Progress of the time-averaged dissolved oxygen concentration obtained by CFD for configurations G1 and G2 as a function of developed helix length, showing conditions C2, C13 and C18 for G1 and C2, C3 and C13 for G2, respectively. Triangles denote corresponding experimental measurements using oxygen probes in geometry G1.

such conditions. Kashid et al. (2011) showed for different flow regimes in microchannels an increasing liquid-liquid mass transfer rate with increasing liquid flow velocities. For gas-liquid mass transfer in straight tubes it is known, that the mass transfer increases with increasing flow velocities when the flow regime changes from bubble, to annular, to annular-spray flow (Charpentier, 1981). Therefore, it should be possible to enhance the mass transfer rate further if the velocities are increased, reaching other flow regime.

The results of this study show that the helical geometry ensures good mass transfer in two-phase flows, with low axial backmixing. Therefore, the helix geometry is suitable as a promising chemical reactor geometry to support gas-liquid reactions. Due to the coiling the helix reactor is very compact with a high surface to volume ratio ensuring good heat transfer. A drawback of the coiling is the higher pressure loss. However, this can also be an advantage, as the pressure loss can lead to an over-saturation of the liquid-phase. Controlling the flow regime can help to get optimal conditions, opening the door for higher yields and selectivities in multi-phase reaction systems.

7. Conclusions

Mass transfer and backmixing of air-water flow in the elongated bubble flow regime through a horizontal helically coiled tube reactor have been studied using different experimental and numerical approaches. Two coil configurations (G1 and G2) with different curvature ratios have been used for the experiments and the CFD modeling. In G1 a detailed study of the mass transfer and backmixing behavior was done, using 16 cases with different gas- and liquid-flow rates. For the experimental study in G2 four cases have been selected. In G1 oxygen optodes where used, whereas the study in G2 was done with an optical measurement technique and an oxygen-sensitive dye.

The mass transfer in G1 shows an increasing mass transfer rate with increasing gas and liquid volumetric flow rates. In both G1 and G2, an increasing mass transfer rate is observed when the gas hold-up increases. The axial dispersion increases with higher $Re_{s,G}$, but decreases with a higher superficial velocity of the liquid-phase. This behavior of the two-phase flow is different from previous studies considering only dispersion in the liquid-phase. Correlations for mass transfer and Bodenstein numbers have been proposed.

The mass transfer was also modeled with CFD, involving a Gas Dissolution Model. The numerical results in

excellent agreement with the experimental results.
With the proposed two-phase dispersion model it is possible to describe the residence time behavior of flow through the coiled reactor.
Based on the CFD results, it can be concluded that the curvature ratio has a big influence on mass transfer. A smaller curvature ratio promotes mass transfer between the phases. Overall, the results of this study show that the mass transfer rate withing the coiled reactor is good and the system exhibits a relatively low axial dispersion effect.

8. Acknowledgment

This work is part of the Collaborative Research Center/ Transregio 63 "Integrated Chemical Processes in Liquid Multiphase Systems" (subproject B1). Financial support by the Deutsche Forschungsgemeinschaft (DFG, German Research Foundation) is gratefully acknowledged (TRR 63).

The authors would like to thank P. Kováts and D. Koós for their help concerning experiments and post-processing in geometry G2.

Bibliography

References

Abdel-Aziz, M., Mansour, I., Sedahmed, G., 2010. Study of the liquid-solid mass transfer controlled processes in helical tubes under turbulent flow conditions. Chemical Engineering and Processing 49, 643–648.

Ali, S., 2001. Pressure drop correlations for flow through regular helical coil tubes. Fluid Dynamics Research 28, 295–310.

Austin, L. R., Seader, J. D., 1975. Entry region for steady viscous flow in coiled circular pipes. AIChE 20, 820822.

Baerns, M., Behr, A., Brehm, A., Gmehling, J., Hoffmann, H., Onken, U., Renken, A., 2006. Technische Chemie, 1st Edition. Wiley-VCH.

Banerjee, S., Rhodes, E., Scott, D., 1970. Studies on cocurrent gas-liquid flow in helically coiled tubes II: Theory and experiments on turbulent mass transfer with and without chemical reaction. The Canadian Journal of Chemical Engineering 48, 542–551.

Charpentier, J., 1981. Mass-transfer rates in gas-liquid absorbers and reactors. Advances in Chemical Engineering 11, 1–133.

Darzi, A., Farhadi, M., Sedighi, K., Aallahyari, S., Delavar, M., 2013. Turbulent heat transfer of Al2O3-water nanofluid inside helically corrugated tubes: numerical study. International Communications in Heat and Mass Transfer 41, 68–75.

Epstein, P., Plesset, M., 1950. On the stability of gas bubbles in liquid-gas solutions. J. Chemical Physics 18, 1505.

Ferng, Y., Lin, W., Chieng, C., 2012. Numerically investigated effects of different Dean number and pitch size on flow and heat transfer characteristics in a helically coil-tube heat exchanger. Applied Thermal Engineering 36, 378–385.

Fsadni, A., Whitty, J., 2016. A review on the two-phase heat transfer characteristics in helically coiled tube heat exchangers. International Journal of Heat and Mass Transfer 95, 551–565.

Grachia-Ochoa, F., Gomez, E., 2009. Bioreactor scale-up and oxygen transfer rate in microbial processes: An overview. Biotechnology Advances 27, 153–176.

Hameed, M., Muhammed, M., 2003. Mass transfer into liquid film falling in straight and helically coiled tubes. International Journal of Heat and Mass Transfer 49, 1715–1724.

Han, L., Al-Dahhan, M., 2007. Gas-liquid mass transfer in high pressure bubble column reactor with different sparger designs. Chemical Engineering Science 62, 137–139.

Hofmann, H., 1961. Der derzeitige Stand bei der Vorausberechnung der Verweilzeitverteilung in technischen Reaktoren. Chemical Engineering Science 14, 193–208.

Ito, H., 1959. Friction factors for turbulent flow in curved pipes. J. Basic Eng. 81 (2), 123–134.

Jayakumar, J., Mahajani, S., Mandal, J., Vijayan, P., Bhoi, R., 2008. Experimental and CFD estimation of heat transfer in helically coiled heat exchangers. Chemical Engineering Research and Design 86 (3), 221–232.

Jepsen, J., 1970. Mass transfer in two phase flow in horizontal pipelines. AIChE Journal 16, 705–711.

Ju, H., Huang, Z., Xu, Y., Duan, B., Yu, Y., 2001. Hydraulic performance of small bending radius helical coil-pipe. Journal of Nuclear Science and Technology 38 (10), 826–831.

Kashid, M., Renken, A., Kiwi-Minsker, L., 2011. Influence of flow regime on mass transfer in different types of microchannels. Industrial & Engineering Chemical Research 50, 6906–6914.

Kulic, E., Rhodes, E., 1974. Chemical mass transfer in co-current gas-liquid slug flow in helical coils. The Canadian Journal of Chemical Engineering 52, 114–116.

Kumar, V., Saini, S., Sharma, M., Nigam, K., 2006. Pressure drop and heat transfer study in tube-in-tube helical heat exchanger. Chemical Engineering Science 61 (13), 4403–4416.

Levenspiel, O., 1998. Chemical Reaction Engineering, 3rd Edition. John Wiley & Sons.

Levenspiel, O., 2012. Tracer Technology: Modeling the flow of fluids, 1st Edition. Springer Science+Business Media, LLC 2012.

Malgorzata, N., Piotr, L., 2014. Probe dynamics influence on determination of volumetric oxygen transfer coefficient. In: 19th International Conference on Methods and Models in Automation and Robotics (MMAR). IEEE, pp. 395–400.

Mandal, S., Das, S., 2002. Gas-liquid flow through helical coils in horizontal orientation. The Canadian Journal of Chemical Engineering 80, 979–983.

Mandhane, J., Gregory, G., Aziz, K., 1974. A flow pattern map for gas-liquid flow in horizontal pipes. International Journal of Multiphase Flow 1, 537–553.

Merchuk, J., Yona, S., Siegel, M., Ben Zvi, A., 1989. On the first order approximation to the response of dissolved oxygen electrodes for dynamic $k_l a$ estimation. Biotechnology and Bioengineering 35, 1161–1163.

Mills, A., 2005. Oxygen indicators and intelligent inks for packaging food. Chemical Society Reviews 34 (12), 1003–1011.

Mishra, P., Gupta, S., 1979. Momentum transfer in curved pipes: 1. newtonian fluids. Industrial & Engineering Chemical Process Design and Developement 18, 130–137.

Naphon, P., Wongwises, S., 2006. A review of flow and heat transfer characteristics in curved tubes. Renewable & Sustainable Energy Reviews 10 (5), 463–490.

Rahimi, M., Askari, A., Ghanbari, M., 2014. Hydrodynamics of isothermal upward two phase flows in helical coils. Petroleum and Coal 56 (5), 562–571.

Ranganathan, P., Sivaraman, S., 2011. Investigations on hydrodynam-

ics and mass transfer in gas-liquid stirred reactor using computational fluid dynamics. Chemical Engineering Science 66 (14), 3108–3124.

Reis, N., Pereira, R., Vicette, A., Teixeira, J., 2008. Enhanced gas-liquid mass transfer of an oscillatory constricted-tubular reactor. Industrial & Engineering Chemistry Research 47, 7190–7201.

Rennie, T., Raghavan, V., 2006. Numerical studies of a double-pipe helical heat exchanger. Applied Thermal Engineering 26 (11), 1266–1273.

Rippel, G., Edit Jr, C., Jordan Jr, H., 1966. Two-phase flow in coiled tube. I&EC Process Design and Development 5, 32–39.

Saamito, A., Kurnia, J., Mujumdar, A., 2011. Numerical evaluation of laminar heat transfer enhancement in nanofluid flow in coiled square tube. Nanoscale Research Letters 6 (376).

Saffari, H., Moosavi, R., Nouri, N., Lin, C., 2014. Prediction of hydrodynamic entrance length for single and two-phase flow in helical coils. Chemical Engineering and Processing: Process Intensification 86, 9–21.

Sangani, A., Didwania, A., 1993. Dispersed-phase stress tensor in flows of bubbly liquids at large Reynolds numbers. Journal of Fluid Mechanics 248, 27–54.

Sauer, J., 2000. Instationär kavitierende Strömungen - ein neues Model, basierend auf Front Capturing, VoF und Blasendynamik. Ph.D. thesis, Technische Hochschule Karlsruhe.

Saxena, A., Schumpe, A., Nigam, K., Deckwer, W., 1990. Flow regimes, hold-up and pressure drop for two-phase flow in helical coils. The Canadian Journal of Chemical Engineering 86, 553–559.

Saxena, A., Schumpe, A., Nigam, K., Deckwer, W., 1996. Liquid phase residence time distribution for two phase flow in coiled tubes. The Canadian Journal of Chemical Engineering 74, 861–866.

Shah, A., Sharma, M., 1973. Mass transfer in liquid-liquid coil contractor. The Canadian Journal of Chemical Engineering 51, 772–775.

Sharma, L., Nigam, K., Roy, S., 2017. Axial dispersion in single and multiphasic flows in coiled geometries: Radioactive particle tracking experiments. Chemical Engineering Science 157, 116–126.

Thandlam, A. K., Das, C., Majumder, S. K., 2016. Flow pattern-based mas and heat transfer and frictional drag of gas-non-newtonian liquid flow in helical coil: two- and three-phase systems. Heat and Mass transfer, 1–15.

Trivedi, R., Vasudeva, K., 1975. Axial dispersion in laminar flow in helical coils. Chemical Engineering Science 30, 317–325.

Vashishth, S., Kumar, V., Nigam, K., 2008. A review on the potential applications of curved geometries in process industry. Industrial & Engineering Chemistry Research 47, 3291–3337.

Vashisth, S., Nigam, K., 2009. Prediction of flow profiles and interfacial phenomena for two-phase flow in coiled tubes. Chemical Engineering and Processing: Process Intensification 48 (1), 452–463.

Wang, T., Wang, J., 2007. Numerical simulations of gas-liquid mass transfer in bubble colums with a CFD-PBM coupled model. Chemical Engineering Science 62 (24), 7107–7118.

Wang, X., Dong, H., Zhang, X., Xu, Y., Zhang, S., 2010. Numerical simulation of absorbing CO2 with ionic liquids. Chemical Engineering and Technology 33 (10), 1615–1624.

Whitman, W., 1923. The two film theory of gas absorption. Chemical and Metallurgical Engineering 23, 146–148.

Highlights:

- Different measurement techniques were used to study the gas-liquid mass transfer
- Computational Fluid Dynamics (CFD) was used to model the gas-liquid mass transfer
- The results indicate an influence of the coil curvature ratio on the mass transfer